satisfies the Schrödinger equation and periodicity condition described by $\mathbf{g}$, so does

$$\varphi_{n\mathbf{g}}(-\mathbf{r})^*=u_{n\mathbf{g}}{}^*(-\mathbf{r})\exp(i\mathbf{g}\cdot\mathbf{r}). \quad (B.4)$$

From the assumed nondegeneracy of the $\epsilon_n(\mathbf{g})$ we conclude that

$$u_{n\mathbf{g}}{}^*(-\mathbf{r})=Cu_{n\mathbf{g}}(\mathbf{r}), \quad (B.5)$$

where C is a numerical constant. Setting $\mathbf{r}=0$, we see that $C=1$, so that

$$u_{n\mathbf{g}}(-\mathbf{r})=u_{n\mathbf{g}}{}^*(\mathbf{r}). \quad (B.6)$$

Now let us divide $u_{n\mathbf{g}}$ into a real and imaginary part:

$$u_{n\mathbf{g}}(\mathbf{r})=v_{n\mathbf{g}}(\mathbf{r})+iw_{n\mathbf{g}}(\mathbf{r}). \quad (B.7)$$

Then, by (B.6) we have

$$v_{n\mathbf{g}}(-\mathbf{r})=v_{n\mathbf{g}}(\mathbf{r}), \quad (B.8)$$

$$w_{n\mathbf{g}}(-\mathbf{r})=-w_{n\mathbf{g}}(\mathbf{r}). \quad (B.9)$$

But as the operator

$$p_\alpha\equiv(1/i)(\partial/\partial x_\alpha) \quad (B.10)$$

is odd under inversion we have

$$\begin{aligned}&p_{nn'}{}^\alpha(\mathbf{g})\\&=\frac{(2\pi)^3}{\Omega}\int\varphi_{n\mathbf{g}}{}^*p^\alpha\varphi_{n'\mathbf{g}}d\mathbf{r}\\&=\delta_{nn'}g^\alpha+\frac{(2\pi)^3}{\Omega}\int u_{n\mathbf{g}}{}^*p^\alpha u_{n'\mathbf{g}}d\mathbf{r}\\&=\delta_{nn'}g^\alpha+\frac{(2\pi)^3}{\Omega}\int(v_{n\mathbf{g}}p^\alpha iw_{n'\mathbf{g}}-iw_{n\mathbf{g}}p^\alpha v_{n'\mathbf{g}})d\mathbf{r}, \quad (B.11)\end{aligned}$$

and in view of (B.10) this is clearly real.

At special points $\mathbf{g}$, where either of the conditions mentioned after Eq. (B.2) fails, the property (B.2) will still hold if one chooses $\varphi_{n\mathbf{g}}$ as the limit of $\varphi_{n\mathbf{g}'}$ where $\mathbf{g}'\rightarrow\mathbf{g}$.

PHYSICAL REVIEW VOLUME 115, NUMBER 6 SEPTEMBER 15, 1959

Self-Diffusion and Nuclear Relaxation in He^3

R. L. GARWIN AND H. A. REICH
International Business Machines Watson Laboratory at Columbia University, New York, New York

(Received March 3, 1959; revised manuscript received August 14, 1959)

Direct spin-echo measurements of diffusion coefficient (D) and spin relaxation time (T_1 and T_2) have been performed on He^3, with an accuracy $\sim 2\%$ in the range 0.5°K to 4.2°K and at pressures to 67 atmos in the liquid, the solid, and in dilute solutions of He^3 in He^4. Unactivated diffusion is observed to the lowest temperatures in the liquid, but not in the solid. By measurement of D at 19 atmos we find an activation energy of 13.7°K for the production of scatterers in He II. There is an extended discussion of experimental details.

I. INTRODUCTION

IN order to resolve some questions raised by thermodynamic measurements,[1] we began some time ago an experiment to measure by the spin-echo technique the nuclear susceptibility of pure liquid He^3 and so to exhibit the expected Fermi degeneracy. By the use of spin echoes[2] it is possible to obtain, in addition to the nuclear spin susceptibility, accurate values of the spin relaxation times, transverse T_2 and longitudinal T_1, and also of the diffusion coefficient[2,3] of a He^3 atom among other identical He^3 atoms or in He^4. It is on this last that we concentrated after the cw resonance measurements of the spin susceptibility appeared.[4]

In addition to studying the diffusion of a purely quantum particle among its identical neighbors, we expected to find for dilute solutions of He^3 in He^4 that the He^3 diffusion coefficient (under isothermal conditions with uniform concentrations) would increase rapidly with decreasing temperature below the λ point,[5] and we wanted to exhibit the absence of scattering of He^3 by He^4 at low temperatures.

Since both the actual diffusion coefficient and the spin relaxation time (both in liquid and in solid) are measured accurately ($\sim 2\%$) and independently in this experiment, we have also some information of interest in the general mechanisms of nuclear spin relaxation.[6]

Some examples of qualitative (and hence interesting) questions we hoped to answer are:

[1] Weinstock, Abraham, and Osborne, Phys. Rev. **89**, 787 (1953).
[2] E. L. Hahn, Phys. Rev. **80**, 580 (1950).
[3] H. Y. Carr and E. M. Purcell, Phys. Rev. **94**, 630 (1954); hereafter referred to as CP.
[4] Fairbank, Ard, and Walters, Phys. Rev. **95**, 567 (1954).
[5] Garwin, Kan, and Reich, Proceedings of the National Science Foundation Conference on Low-Temperature Physics and Chemistry, Baton Rouge, Louisiana, 1955 (unpublished).
[6] Bloembergen, Purcell, and Pound, Phys. Rev. **73**, 679 (1948); hereafter referred to as BPP.

(1) Does diffusion persist to 0°K in pure He^3 liquid?
(2) Does diffusion persist to 0°K in pure He^3 solid?
(3) What is the detailed behavior of He^3 in He^4 at temperatures below those required for freezing out excitations? Is there a Fermi degeneracy corresponding to a changed effective mass and the lower number density of the He^3 atoms?
(4) Is there a discontinuity in He^3 diffusion at the solution λ point?

Our early measurements on He^3 were performed with 1 cc STP of gas, but with the reduced price of He^3 we now use 200 cc STP at pressures from the vapor pressure to 67 atmos and at temperatures from 4.2°K to <0.5°K (obtained by a continuous He^3 refrigerator[7]). It is of considerable interest to extend these measurements to temperatures low compared with the Fermi temperature to make comparison with the predictions of the many-body theory of Brueckner[8] and the phenomenological theory of Abrikosov *et al.*[9] This will shortly be accomplished by the use of a continuous demagnetization refrigerator operating with a sink at 0.5°K.[10]

II. METHOD

The only direct method of distinguishing a particle from its identical neighbors is by means of the phase of its nuclear spin precession in an external magnetic field. Fortunately a beautiful and convenient method exists, which was discovered by Hahn[2] at the time of his invention of spin echoes. Not only does this method allow a measurement of the true self-diffusion of atoms or molecules but it is both more accurate and much more convenient than conventional techniques of measuring diffusion.

The full derivation of this method of diffusion measurement is to be found in reference 2 and is extended by Carr and Purcell.[3] We shall just recall the spin echo method pictured in Fig. 1. The sample of spins is placed between the poles of a magnet producing a steady field H_0, which however has some uniform derivative over the sample in the direction perpendicular to H_0. A source of pulsed radio-frequency current is used to produce an rf field of magnitude H_1 at the gyromagnetic frequency $\omega_0=\gamma H_0$, allowing one to produce arbitrary nutations of the spin magnetization, among which the "90°" and "180°" pulses are of particular interest. The application of a 90° pulse to the sample (i.e., one for which

$$\int_{t_p}^{t_p+w}(\gamma H_1/2)dt=\pi/2,$$

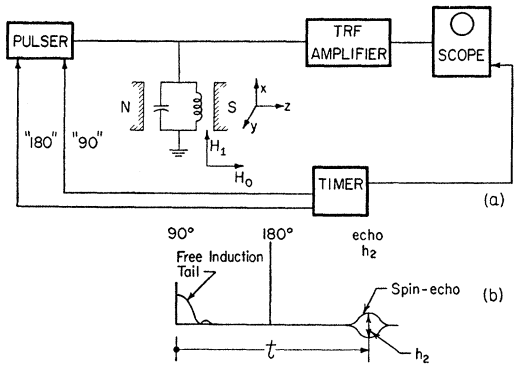

FIG. 1. Simplified schematic of spin echo apparatus. "180" and "90" refer to the precession angle produced by the rf pulse. The spin echo sample is placed inside the coil shown.

where $H_1/2$ is the magnitude of the component of circularly polarized rf field rotating with the spin system, t_p the time of application of the pulse, w its width, γ the gyromagnetic ratio) is followed by an "induction tail," a voltage at frequency ω_0 induced in the coil by the equilibrium (temperature T, field H_0) nuclear spin magnetization precessing about H_0. This induction tail is quenched in a time T^* short compared to the spin relaxation time because spins at different points in the magnet experience different fields H_0, and therefore get out of phase. The shape of the tail depends upon the shape of the sample cell and on the spatial variation of the field H_0. A 180° pulse is never followed by a tail, since the spin system immediately afterwards is just the same as before but inverted with respect to H_0. The sequence of pulses 90° and 180° applied to the spin system initially in thermal equilibrium produces a "spin-echo" at a time after the 180° pulse equal to the time between the 90° and 180° pulse. Neither the 90° pulse, the 180° pulse, nor the combination 180° then 90° produces the slightest trace of an echo since the echo arises from the precession back into phase of the nuclei at various points in the magnet. The precession phase of each of these spins was reversed by the 180° pulse and if each spin remains in the same position in the magnet, they will all come into phase exactly at the same time. Thus the echo shape is that of two induction tails back-to-back. Measurements on the echo do not suffer from amplifier saturation and recovery problems as do those which are done on the induction tail itself, and we therefore measure only echoes, providing always an additional echo at short times so that picture-to-picture comparisons are never made for measurement of the diffusion coefficient or of T_2. In the absence of diffusion, as the time t [Fig. 1(b)] is increased the echo amplitude falls as $h=\exp(-t/T_2)$, thus allowing an accurate determination of the transverse relaxation time T_2, which may range from one microsecond to many seconds. This may be done even though the line width measured in a cw resonance experiment is a million times wider than that corresponding to T_2—that

[7] K. N. Zinov'eva, J. Exptl. Theoret. Phys. U.S.S.R. **34**, 609 (1958) [translation: Soviet Phys. JETP **34**(7), 421 (1958); H. A. Reich and R. L. Garwin, Rev. Sci. Instr. **30**, 7 (1959).
[8] K. A. Brueckner and J. L. Gammel, Phys. Rev. **109**, 1023 (1958).
[9] A. A. Abrikosov and I. M. Khalatnikov, J. Exptl. Theoret. Phys. U.S.S.R. **32**, 1083 (1957) [translation: Soviet Phys. JETP **5**, 887 (1957).
[10] Heer, Barnes, and Daunt, Rev. Sci. Instr. **25**, 1088 (1954).

is, for a sample which is in a very inhomogeneous field H_0 producing a short tail decay time T^* ($T^* \ll T_2$). On the other hand, if the atomic species has a large diffusion coefficient D ($D \equiv d/dt\langle y^2 \rangle$) the spins in their precession after the 180° pulse will experience different fields than before, being in slightly different positions of the magnet, and the echo will be smaller than it would have been from relaxation alone. This effect may be very large (a few milliseconds *versus* many seconds for T_2). It is also the basis for measuring D directly over a remarkably wide range. In fact, in the presence of diffusion,

$$h_2 = \exp(-t/T_2)\, \exp(-\gamma^2 G^2 D t^3/12), \qquad (1)$$

where t is the time between 90° pulse and echo, D is the diffusion coefficient in cm²/sec, $G \equiv \partial H_0/\partial y$ is the uniform variation of H_0 with position over the sample, γ is the gyromagnetic ratio ($\gamma H_0 = \omega_0$), and T_2 is the transverse relaxation time of the spins.

In our case $G \simeq 3$ gauss/cm; 2×10^{-4} sec $\leqslant t \leqslant 200$ sec (the lower time being set by the width of the echoes, the larger by the liquid T_1), and γ for $He^3 \simeq 2\times10^4$ radians/sec gauss. Thus, a large effect (damping by a factor 3 due to diffusion) sufficient to measure D to $<1\%$ may be obtained with the same apparatus for D between 10^{-15} cm²/sec and 500 cm²/sec, truly a remarkable experimental range. Over this entire range the fractional accuracy of the diffusion coefficient is constant, being determined by the accuracy of time delay measurement, the knowledge of the gradient, and the scatter of the data due to noise.

That the diffusion coefficient measured is that of an atom and not simply the "spin-diffusion" due to interaction of neighboring nuclear moments may be seen by observing that the field of one spin at the other is ~ 1 gauss, producing a precession rate $\sim 10^4$ radians/sec, corresponding *with optimum correlation time* to a pure "spin-diffusion" no more rapid than a jump rate 10^4 sec^{-1} to distances $\sim 3\times10^{-8}$ cm. Thus $D_s \equiv \lambda v/3 = \lambda^2/3t \leqslant 3\times10^{-12}$ cm²/sec.

Thus, any D measured to be larger than 3×10^{-12} cm²/sec, as are all the results of this paper, is pure atomic diffusion.

Our spin relaxation times T_1 are frequently long (several minutes) and amplifier gain drift might be a problem in measuring successive echoes, while the comparison of an echo amplitude with that of a 90° tail involves amplifier recovery problems. We therefore use the pulse pattern of Fig. 2 ("90–180–180") which produces automatically two echoes—the first for measurement of initial amplitude h_1, which is a measure

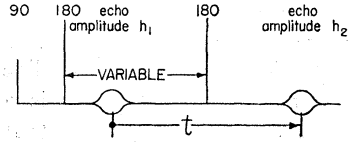

FIG. 2. Pulse sequence used in determination of transverse relaxation time T_2 and diffusion coefficient D. Echoes are shown.

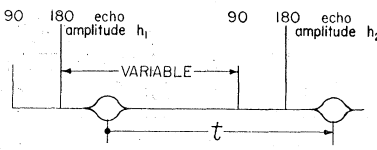

FIG. 3. Pulse sequence and echoes used in determination of longitudinal relaxation time T_1.

of equilibrium magnetization M_0, the second for measurement of the effects of relaxation and diffusion. The sample spin-state at the time of the first echo is exactly the same as it was immediately after the 90° pulse except for a small (and constant) relaxation the effects of which are rigorously negligible. Thus a second 180° pulse produces an echo h_2 as described above and allows us to measure T_2 and D. In this case Eq. (1) describes the time dependence of the ratio h_2/h_1, where t is now the time between the echoes. For liquid He^3, T_2 damping [Eq. (1)] is substantially negligible during the time t in which the echo is observed to decay, and a single measurement of the ratio h_2/h_1 yields D to $\sim 1\%$. Actually, if T_2 is exceedingly short, as in the case of the α-phase of solid He^3, it may be difficult to determine the additional damping due to D and vice versa. The damping due to D may be reduced either by reducing G or by applying a method due to Carr and Purcell[3] which was derived by us independently[11] for the purpose of testing for damping due to convection.

The longitudinal spin relaxation time T_1 (spin-lattice relaxation time) is measured with our two-echo philosophy by applying the pulse train shown in Fig. 3 ("90–180–90–180"), where the second pair of pulses is moved as a unit with respect to the first and now

$$h_2/h_1 = 1 - e^{-t/T_1}. \qquad (2)$$

Thus, two photographs at different delays allow one to compute T_1 to high accuracy. The "null method" of T_1 measurement of CP could also have been used, but offered no advantage in the present case.

In practice, because of the rather large field gradient required for our diffusion measurements, it is necessary to use narrow rf pulses to insure equal Fourier components of H_1 for each spin frequency ω. These narrow pulses are obtained by discharging a condenser into the resonant circuit, condensers charged to different voltages being used for the 90° and the 180° pulse. Since the sample diameter is 6 mm and the gradient ~ 3 gauss/cm, the spin spectrum is 6 kc wide, while with our H_1 rf pulse of exponential envelope with a decay time ~ 2 microseconds the rf field spectrum extends to 80 kc and is flat to $<1\%$ to 10 kc. The H_1 peak amplitude for the 180° pulse is ~ 160 gauss.

Since the echo width is ~ 300 microseconds, while the time between the two echoes of a single pulse train is as long as 200 seconds, one would have great difficulty seeing the echoes at all at a scope beam intensity which

[11] Anderson, Garwin, Hahn, Horton, Tucker, and Walker, J. Appl. Phys. **26**, 1324 (1955).

did not completely fog the film. We have, therefore, triggered the sweep once for each echo at time $t_2 \simeq 500$ microseconds before the echo is expected, thus displaying the details of each echo, which are photographed superimposed. The scope displayed the actual unrectified rf to insure linearity of the system.

III. APPARATUS

A. Cryogenics

The Dewars used to reach 1.2°K were of conventional all-metal design, with extended tail assembly 2-in. o.d. and $1\frac{1}{4}$-in. i.d. reaching into the center of the resonance magnet. Attached to the nitrogen bath was a copper tail for radiation shielding of the He^4 bath which was contained in the inner tailed Dewar. A guard vacuum was used between He^4 and N_2 Dewars separate from that which isolated the N_2 Dewar from the outer jacket to allow quick cooling of the inner Dewar if the occasion demanded. The N_2 Dewar was refilled automatically by an N_2 level control and had an evaporation rate of 0.5 liter per hour. The 1.5-liter He^4 Dewar with the experimental apparatus inserted had an evaporation rate at low temperature of 0.1 liter per hour. Temperatures to ~1.2°K were reached by means of a 46 cfm Kinney pump located in the next laboratory and connected by 6-in. diam tubing. Temperatures between 0.5°K and 1.2°K were readily obtained by the use of a small Welch pump modified to act as a continuous He^3 refrigerator,[7] using 80 cc STP of He^3.

Adequate temperature control was achieved by means of a mercury manostat in the high-temperature range (above 1 cm Hg pressure) and by manipulation of throttle and bypass valves in the low range. Secondary carbon resistance thermometers (Allen-Bradley $\frac{1}{10}$ watt and Speer Carbon Company $\frac{1}{4}$ watt) were calibrated against the vapor pressure of liquid He^4 using the T_{55E} scale. A calibration was performed upon each cooling of the apparatus. The drifts were significant for the Speer but negligible for the Allen-Bradley resistors. Resistance values were measured on a 100 cps Wheatstone bridge constructed for the purpose and yield temperatures accurate to 5 mdeg. The sensitivity was, of course, much higher. Temperatures below 1.1°K were determined by extrapolation, using the 3 constant formula of Clement and Quinnell.[12] Different thermometers indicate the same temperature upon extrapolation, when in thermal equilibrium at 0.5°K. The estimated uncertainty due to systematic errors is <0.010°K at 0.5°K.[13]

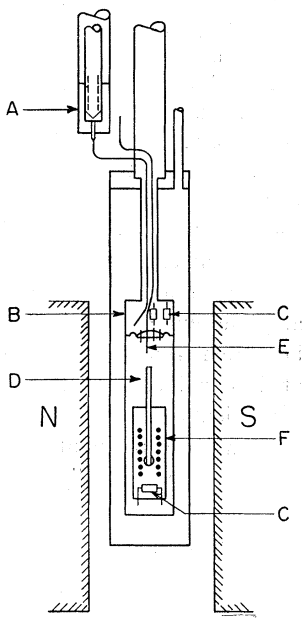

FIG. 4. Schematic of low temperature apparatus. The helium Dewars are of conventional design and are not shown. *A*—needle valve used to control continuous flow of He^3 to *B*—evaporator, where cooling to 0.5°K takes place. *C*—carbon resistance thermometers and heater. *D*-isothermal space filled at room temperature with 1 atmos of He^4. *E*—filling capillary for space *D*. *F*—sample cell. Not shown are the leads to the sample cell and resistance thermometers.

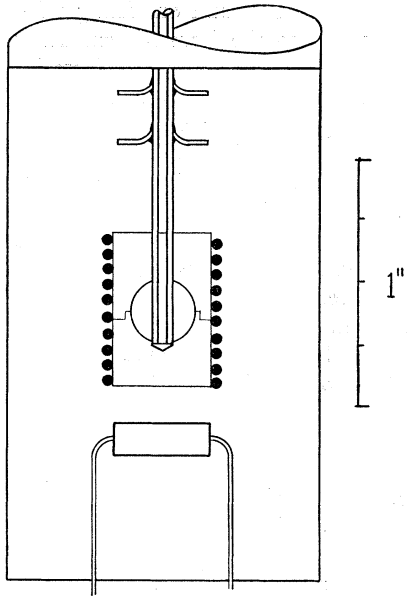

FIG. 5. He^3 sample cell. The rf coil is wound on a split Araldite form (parting line shown), the filling tube is inserted and the assembly is cast into the shape shown.

The experimental apparatus inserted within the He^4 Dewar is shown in Fig. 4. One can see that all leads are brought in through either He^4 or He^3 gas, the needle valve (*A*) and refrigerator section (*B*), the sensing and heating resistors (*C*) in the refrigerator space for use with an automatic temperature regulator not yet needed. Below the refrigerator section is a region (*D*) filled with He^4 through a capillary (*E*) to insure good thermal contact between the sample cell (*F*) and the refrigerator. Starting from 77°K one could reach 1.2°K within 20 minutes and 0.5°K in five minutes more.

B. Sample Cell

The sample cell, Fig. 5, is made of cast araldite, Ciba No. 502. It is fabricated in two pieces (parting line

[12] J. R. Clement and E. H. Quinnell, Rev. Sci. Instr. **23**, 213 (1952).
[13] N. Kurti (private communication).

indicated), the coil is wound on, filling tube inserted, and is then cast into the form shown. The two disks (2-mil copper foil) on the filling tube form feather-edge seals, and are necessary to prevent leaks which otherwise appear upon recycling several times (slowly, to prevent cracking) to low temperatures and high pressures. The sample cell is tight to superfluid helium in either direction at high pressure. It will withstand an internal pressure of 2000 psi at room temperature, and probably a higher pressure when cold, although this has not been tested. The copper filling tube is used to insure isothermal conditions in the bulk of the liquidl in view of the low thermal conductivity.[14] A carbon resistance thermometer is cast into the block just below the coil for purposes of monitoring the temperature as close as possible to the liquid. Presumably because of strain effects, the calibration curve of this resistor is quite different from that of all others. Upon applying rf pulses a transient heat pulse can be observed, which dies away in less than one second, thus giving an order of magnitude for the time required to reach therma, equilibrium. The thermal relaxation time of the He^3 sample, calculated from the thermal diffusivity $K/\rho c$ and the known geometry is ~ 5 seconds, for $0.2°K < T < 4°K$.

Following the lead of Low and Rorschach, we have more recently employed cells machined from nylon bar. Gas seals are made by machines brass cones, which employ the differential thermal contraction to aid the seal. These cells survive repeated chilling in liquid nitrogen, withstand 5000 psi, and are easier to make.

C. Pressure System

Pressures are generated by a Mansfield and Green[15] dead-weight pressure unit, which is guaranteed to have $\frac{1}{4}\%$ accuracy. This unit is used to compress oil, which in turn pushes mercury into a steel Toepler-like gas compressor. To prevent entrance of mercury into the low-temperature region the level is monitored by means of a thick-walled glass capillary tube which has been tested to 5000 psi, and by an electrical alarm relay. A monel capillary, 0.020 o.d.$\times$0.008 i.d., carries the compressed gas to the low-temperature sample cell. Dead volume is minimized by filling the capillary with 0.008-in. wire. Care is taken to allow no ferromagnetic or superconducting materials near the sample.

D. Gas Handling System

The He^3 gas, of which 200 cc STP was required to fill the apparatus with solid at 67 atmos, is stored in a glass gas-handling system equipped with a conventional glass Toepler pump. Dilute mixtures with He^4 are obtained by mixing known pressures of the gases at the same volume, and the gas is admitted to the experimental system through a liquid-helium cooled trap.

[14] Lee, Donnelly, and Fairbank, Bull. Am. Phys. Soc. Ser. II, **2**, 64 (1957).
[15] Mansfield and Green Company, Cleveland, Ohio.

E. Electronics

Magnet.—The magnet is a small homemade electromagnet with a 3-in. diam yoke and 6-in. diam pole pieces. The gradient was obtained by a $\frac{1}{32}$-in. aluminum shim at one side of the 2-in. gap. The magnet was operated at $\sim$1600 gauss ($\sim$6 amperes at 20 volts) and was stabilized to $\sim$1 ppm by a transistorized current regulator.[16] A transistorized quartz-crystal- controlled nuclear resonance marginal oscillator[17] was used with a glycerin sample in a fixed monitor position to adjust the field to the desired value. It was customary to tune the entire apparatus when cold, admit the He^3, and to photograph a perfect echo of maximum amplitude without having previously seen the He^3 nuclear resonance. This ability was necessary since the relaxation time of the liquid was several minutes, and one had no chance to adjust parameters while searching for the He^3 echo.

Spin-echo electronics.—The spin-echo apparatus was required to generate appropriate complex trains of 90° and 180° pulses with delay times varying from 100 microseconds to 10 seconds, to give scope trigger pulses accurately 500 microseconds before each echo was expected, to displace the two echoes (vertically) on the display, and to amplify linearly and with good noise figure the spin-echo signal itself.

The rf amplifier which serves to amplify the spin-echo signal for presentation on the scope is of conventional design, except for a few details shown in Fig. 6 (receiver and transmitter). The input stage is of the cascode type for good noise figure, and the tuned circuit in the cryostat has as high a Q as was obtainable with the long leads to the sample cell, which must carry the rf with little loss but not contribute too much heat leak. We have used in the past gold- or copper-plated Constantan wire and now use Litz wire, yielding a $Q \sim 30$. Most of the resonant capacitance is at helium temperatures to reduce losses. The resonant impedance is chosen to be $\sim$10 000 ohms for best signal-noise ratio. A larger impedance would diminish s/n due to "induced grid noise," a smaller because of shot noise. The impedance is purposely matched for best s/n and *not* for maximum power transfer. The single long RC time constant at the receiver input insures that the grid-cathode diode of the input stage does not load the ringing of the sample coil after the first half-cycle. Two stages of the amplifier employ remote cutoff tubes, and the gain can be varied from 1.5×10^4 to 1.5×10^2. Typical h_1 echoes at 1°K induce a signal of $\sim$0.1 mv in the coil. The equivalent noise temperature is 50°K. The rf amplifier is used with a resonant output into a Tektronix 535 oscilloscope set usually at 1 volt/cm. A convenient test of receiver gain and stability is provided by coupling into the sample coil through a 0.1-mmf condenser a

[16] R. L. Garwin, Rev. Sci. Instr. **29**, 223 (1958).
[17] Garwin, Patlach, and Reich, Rev. Sci. Instr. **30**, 79 (1959).

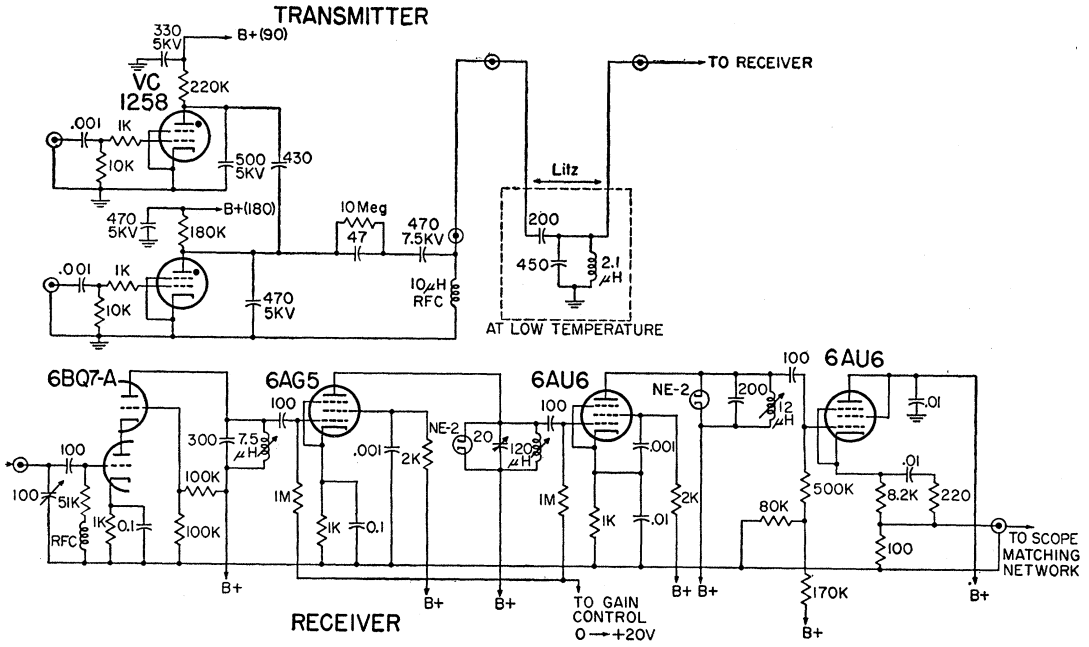

FIG. 6. Schematic of spin echo transmitter and receiver. The energy storage capacitors shown in the transmitter have been chosen to make the plate voltage approximately equal for both 90 and 180. Filament, screen, and plate decoupling networks to avoid oscillation are of conventional design and are not shown in the receiver. The scope matching network is a simple T, chosen to match the low line impedance to the high scope impedance. It has a gain of 10.

few-volt step function from a mercury-switch pulse generator.[18]

The transmitter consists of a pair of miniature hydrogen thyratrons VC 1258.[19] each of which discharges its charging condenser into the tuned circuit. The pulse amplitudes for 90° and 180° are adjusted independently by varying the high-voltage to the thyratrons. Since the receiver input noise voltage is about a microvolt, one must be very careful about noise from the thyratrons while they are deionizing and from the other circuit elements which have just been subjected to a two-kilovolt pulse. The thyratrons are noiseless after a few microseconds, but one must use for the dc-blocking condenser a 7.5-kv ceramic condenser to avoid large noise pulses from the condenser itself. The actual pulse coupling condensers have dc voltage for only a few microseconds and contribute no noise pulses after 50 microseconds. Note that we vary here the magnitude of H_1 and not its duration, contrary to the usual spin-echo practice. The exponentially decaying rf pulse is just as effective as the more usual square pulse, having a Fourier spectrum $[1+\tau^2(\omega-\omega_0)^2]^{-1}$ rather than $[\tau(\omega-\omega_0)]^{-1}\sin\tau(\omega-\omega_0)$ where τ is the exponential damping time or the pulse half-width. It should be noted that the transmitter is *incoherent*, which causes no trouble with the proper echoes to be measured.

Pulse timing and sequencing.—Four delays suffice to make the measurements of diffusion and relaxation considered here. For the T_2 and D measurements they are shown in Fig. 7(a), together with a block diagram of the pulse generators [Fig. 7(b)]. The corresponding diagram for T_1 is shown in Fig. 8. The various times are:

t_0—a fixed delay, usually about 0.4 msec to obtain a first echo not much damped by diffusion or relaxation.

t_2—a delay of 0.5 to 1.0 msec, which serves to trigger the scope twice at a time t_2 before each echo. This enables the echoes to be displayed in full detail, as in Fig. 12(a).

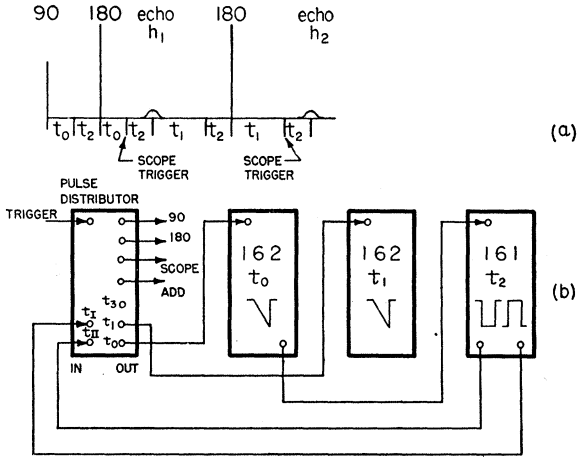

FIG. 7. (a) Timing scheme, and (b) block diagram to produce 90–180–180 sequence. $t_0=0.4$ msec, $t_2=0.5$ msec, t_1 variable from 0.5 msec to 10 sec. t_2 is chosen to center the echo on the oscilloscope sweep.

[18] R. L. Garwin, Rev. Sci. Instr. **21**, 903 (1950).
[19] Chatham Electronics, Newark, New Jersey.

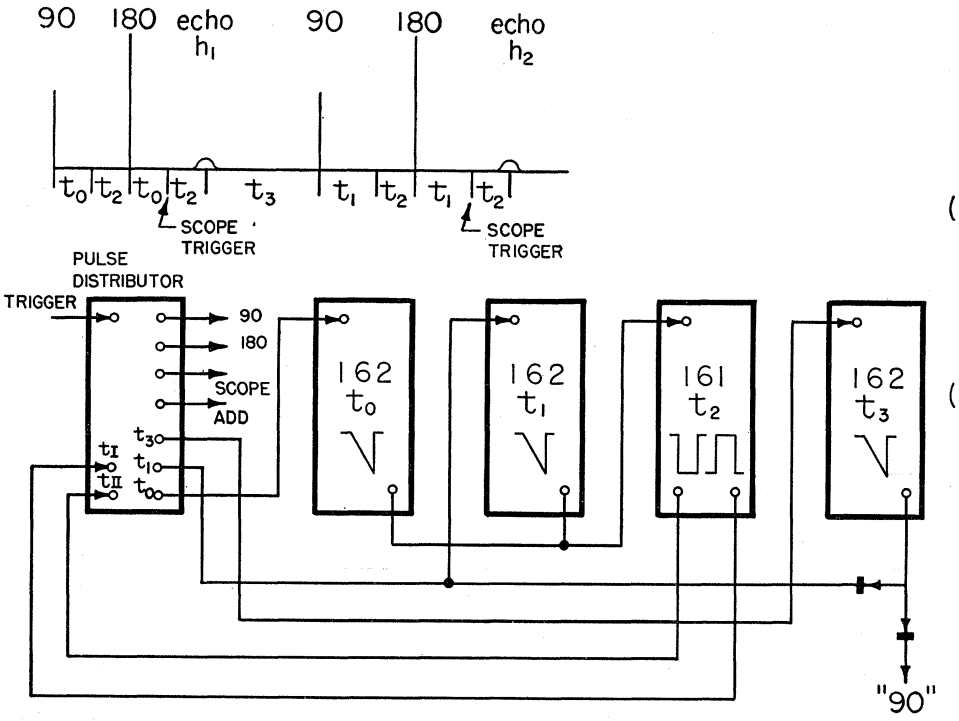

FIG. 8. (a) Timing scheme, and (b) block diagram to produce 90–180–90–180 sequence. t_0 = 0.4 msec, t_2 = 0.5 msec, t_1 = 0.6 msec. t_3 may be as large as 10 seconds.

t_1—variable in T_2 or D measurements from 0.5 msec to 10 sec to allow transverse relaxation or diffusion. In T_1 measurements t_1 is about 2.0 msec to obtain an echo not much damped by diffusion or relaxation but at a delay different from t_0. This avoids spurious superpositions in case pulses are not exactly 90° or 180°.[11]

t_3—variable from 1.0 msec to 10 sec. Used in T_1 measurement of pure solid He^3 to allow partial recovery of equilibrium magnetization.

The rather peculiar repeated time intervals were chosen so that we might use Tektronix series 160 time interval generators rather than digital counters which were not at hand at the time. Since the second echo in the T_2 or D measurement is well off the scope if the second t_1+t_2 precession interval is 0.1% different from the first, the only convenient way of obtaining this equality is to trigger the same pulse generators twice. The system used was very convenient since for T_2 or D measurements only t_1 needed to be varied, leaving t_0, t_2, and the scope sweep speed unchanged. Similarly for T_1 measurement only t_3 was varied. The distribution of triggers to the various delay generators, rf pulse generators, scope trigger, scope beam shift, etc. was accomplished by a simple thyratron ring driving a diode matrix pulse distributor. A transistor ring, glow counter or core counter would have done as well, but would have required amplification in order to trigger the rf pulse thyratrons and delay generators. Four conventional blocking oscillators (not shown) were available for producing sharp trigger pulses from the slow rise at the end of long delays from the Model 162 pulse generators. The only time which enters sensitively into the measurements is that between the two echoes; and rather than calibrate the delay generators each time, we have made use of a digital counter[20] which measures the time interval between the two oscilloscope sweeps to an accuracy better than 0.01%. The interval to be measured is simply obtained by connecting to the "gate-output" terminal on the scope and is thus exactly the time t in Eq. (1) or (2).

IV. TECHNIQUE

A. Cryogenic

Before making a run, the He^4-N_2 and N_2-case vacuum spaces were evacuated with a diffusion pump and liquid N_2 admitted to the N_2 reservoir which was thereafter maintained full by an automatic N_2 level control. N_2 was admitted to the He^4-N_2 and He to the He^3-He^4 spaces to a pressure $\sim$100 μ, which brought the inner Dewar to N_2 temperature in a few hours, after which the He^4-N_2 space was pumped with the diffusion pump. In $\sim$30 minutes the He^4 transfer was begun using $\sim\frac{1}{2}$ psi pressure on the He^4 storage Dewar. About 4 liters of He^4 is expended in collecting 1.5 liters of He^4 in the experimental Dewar, sufficient for more than ten hours work. Refills are made with $\sim$1.7 liters each. The apparatus warms to about 20°K overnight, and thus succeeding runs are very economical. A few minutes after filling the sample cell is at 4.2°K,

[20] Type 524-*B*, Hewlett-Packard Company, Palo Alto, California.

at which time the vapor pressure—carbon resistor calibrating run is made. If temperatures $<1.1°K$ are to be used, the He^3-He^4 guard space is pumped with the diffusion pump for ~ 20 mean pressure time constants as measured by an ionization gauge attached to the diffusion pump. The guard vacuum is isolated from the pumps and the system brought by the He^3 refrigerator to the desired temperature. At this time the sample He^3 is transferred into the pressure system through a He^4-cooled capillary. Normally the sample He^3 is kept in the high-pressure system. The sample He^3 is now ready to be condensed and to be compressed by the dead-weight gauge tester.

B. Electronic

Before transferring helium the magnet current regulator[16] is switched on and power applied. Within a few seconds the field is stable as seen by the crystal-controlled proton resonance monitor[17] (which has a press-to-measure switch and normally draws no current from its battery but displays the proton resonance instantly upon depressing the switch). The electronics is turned on, the pulse train is monitored to determine that no tubes have burned out, the receiver input (the sample coil) is tuned by the injection of a small crystal-controlled 5.224 Mc/sec signal which is maximized on the scope by adjustment of the receiver input tuning condenser. If modifications have been made to the resonant circuit, it is necessary to adjust the 90° and 180° pulse amplitude, which can be done *a priori* by comparison with the calibrator response; but it is performed most conveniently by cooling the apparatus and raising the He^3 pressure to produce solid He^3, on which the effects of pulse amplitude may be observed visually since the solid spin relaxation time is a few tenths of a second rather than the 100 seconds liquid relaxation time. A proper setting of 90° and 180° amplitude may be made in the usual way—absence of induction tail on 180° pulse, the absence of induction tail following the second 90° pulse of a pair or, best of all the absence of extra echoes due to 3 arbitrary rf pulses.[11,21] Amplifier recovery time prevents observation of these tails, so a further "180°" pulse is used to convert the tail into an echo at a time not subject to interference. Figure 9(a) shows the nuclear spin-echo response for proper tuning and pulse amplitudes, and 9(b) for wrong pulse amplitudes. Incorrect pulse amplitudes cause no error in the measurements, since one measures at all times only the incremental attenuation due to additional delay.

Some of the spurious echoes are of the so-called "stimulated" type[2,11,21] which decay not in time T_2 but in time T_1, and so can persist several minutes to

[21] For a discussion of the echoes due to 3 rf pulses of arbitrary amplitudes, see for example A. Lösche, *Kerninduktion* (VEB Deutscher Verlag der Wissenschaften, Berlin, 1957), Chaps. 2 and 3.

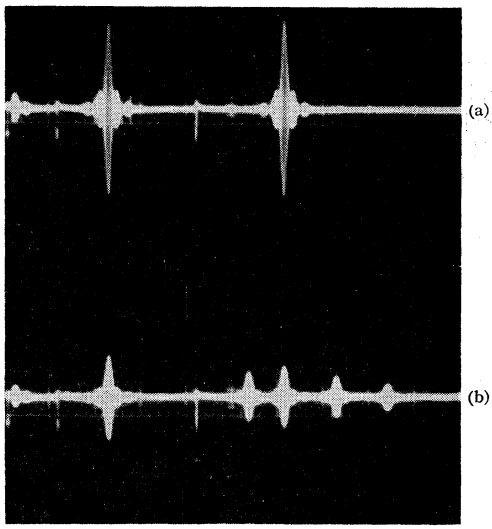

FIG. 9. (a) Photograph of spin echoes resulting from 90–180–180 sequence. The second echo is not much damped by diffusion. (b) Photograph of spin echoes from same pulse sequence as in (a) but with 180 pulse amplitude reduced by half. Notice the diminution of echo amplitude, as well as the appearance of three extra echoes. Sweep speed in both pictures is 1 msec/cm.

cause interference with the echo amplitude on the measurement of the next point. We avoid such difficulties by choosing t_0 different from t_1. These unwanted echoes can also be eliminated by a small pulse of current in a wire near the sample coil.[11] Since our successive rf pulses are incoherent, an echo which is the sum of signals from two or more echoes ("mirror" plus "stimulated" for instance) will have an amplitude which fluctuates on successive measurements, and such falsified echoes may be identified in this manner. The analysis of superposed echoes is complicated, and we avoid such circumstances.

In measuring T_1 there appears to be no substitute for having t comparable to T_1 if the equilibrium signal amplitude is also unknown, but in measuring D or T_2, one can avoid waiting between pictures for times long compared to T_1 ($\sim$5–10 minutes) by *saturating* the spin sample with several ($\sim$10) 90° pulses after a measurement, then waiting a standard time ($\sim$1 minute) before taking the next point on the h_2/h_1 *vs* t curve. This avoids the superposition of false (stimulated) echoes from the previous measurement. In the measurement of T_1, which can be as large as 900 seconds in dilute solutions, the following procedure was used to gain a maximum amount of information per picture, using the 90–180–180 scheme. After saturating the spins, various times, such as 60, 120, 240, $\cdots$ seconds were allowed to elapse. The pulse sequence 90–180–180 was then applied, with differing times between the 180 pulses for each picture. The echoes h_1 hence give us information regarding T_1, while the ratio h_2/h_1 enables D to be determined from a single picture.

C. Recording

The two traces containing the two echoes of amplitude h_1 and h_2 are recorded (superimposed or displaced vertically as desired) on Polaroid film, 3 measurements to a film. The pictures are processed, inspected for the relevant quantities—order of magnitude of T_1 and of the time t at which the echo begins to die, in order to obtain further points in the more significant regions of the decay curve. The points are spaced uniformly in t^3, out to values of t such that h_2 is approximately equal to the noise. This is done instead of taking several points clustered about the value of t for which $h_2/h_1 \sim 0.5$ because of the necessity for determining an additional parameter of the decay curve (the zero intercept). This is usually less than 1, because of improper pulse size. Pulses less in amplitude than "180°" are sometimes intentionally used to avoid gas discharges which may appear at low pressures. A broad spacing of points in t^3 also permits the calculation of T_2 and gives evidence of the absence of convective spin damping.

The photographs are then measured, using a Wilder Microprojector equipped with a micrometer stage. The echo amplitudes, less baseline and noise, and the resulting double amplitudes (in mils) are entered in the data book.

D. Data Reduction

An IBM-650 computer was used with a general purpose iterative least-squares program[22] to perform all the computation associated with the experiment. This is done not so much because of the additional accuracy attained by the least-squares method with more data points than parameters, but mainly because we have in this way a routine method for finding

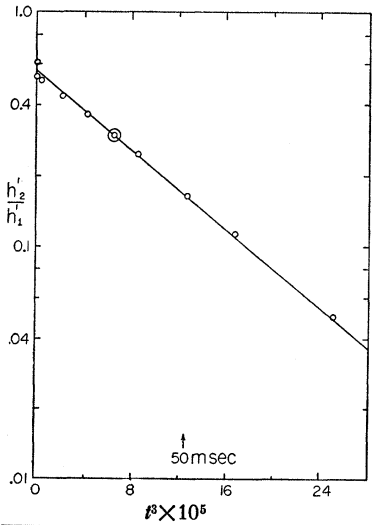

FIG. 10. Plot of h_2/h_1 *vs* t^3 showing decay due predominantly to diffusion.

[22] R. L. Garwin and H. A. Reich, *Mathematics Tables and Other Aids to Computation* (to be published).

experimental or computational blunders. To this end, we fit for Eq. (1) a function

$$y_2^m = h_1^m A \exp(-t_m/T_2 - \gamma^2 G^2 D t_m^3/12), \qquad (3)$$

with m referring to the mth data point at that temperature and pressure. A should be unity for rf pulses exactly 90° and 180° (Fig. 10) and usually is computed to be ~0.90. T_2, A, and D are, however, left free to be adjusted by the 650 for minimum $\sum_m (h_2^m - y_2^m)^2$. More than 90% of the runs have $\sum_m (h_2^m - y_2^m)^2 \leqslant 40$ $(m-2)$ mil^2, the rest having $\sum_m \delta^2$ very much larger due to blunders and errors. Since the echo amplitude is usually ~800 mils it is evident that a measurement accuracy, linearity, noise-to-signal, etc. much better than 1% is routinely achieved. A similar computation is carried out for Eq. (2), fitting now

$$y_2^m = h_2^m[1 - B \exp(-t/T_1)], \qquad (4)$$

with $B \sim 1$, and B and T_1 free. Of course, the damping due to D may be negligible compared to that due to T_2,

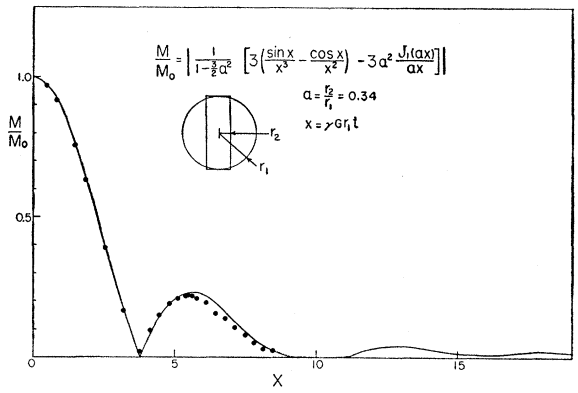

FIG. 11. The line is the theoretical echo shape shown in the equation. The circles are experimental points derived from a typical picture, adjusted to fit the curve by choice of the field gradient G, which is thereby determined.

but the least-squares solution gives also the errors in the parameters.

The same program with a different subroutine is used to determine the best calibrating function for the resistance thermometry.

E. Echo Shape

The shape of the spin echo signal is that of two "tails", back-to-back. The detailed behavior in time of the decay of a "tail" is given by CP Eq. (4). For our case, where we have a cylindrical portion excluded from a spherical sample, we can evaluate the contributions from the cylindrical and spherical parts separately, and then subtract, taking into account the fractional volume of the cylinder. The contribution due to the sphere is $M_s(t) = M_0^3[\sin x/x^3 - \cos x/x^2]$, where $x = \gamma G r t$ and r is the radius of the sphere. M_0 is the total spin magnetization. The contribution from the cylinder is

$M_c(t)=M_0[2J_1(y)/y]$, where $y=\gamma Gr't$ and r' is the radius of the cylinder. Combining these two equations, and taking into account the fractional volume of the cylinder in the approximation $r'\ll r$, we obtain

$$\frac{M(t)}{M_0}=\frac{1}{1-\frac{3}{2}a^2}\left[3\left(\frac{\sin x}{x^3}-\frac{\cos x}{x^2}\right)-\frac{3a^2J_1(ax)}{ax}\right], \quad (5)$$

where $a\equiv r'/r$. The factor in front of the square brackets normalizes M/M_0 to unity at $x=0$. A plot of Eq. (5) is given by the solid line of Fig. 11. The circles are experimental points. In plotting the experimental points, correction has been made for the spot width of the oscilloscope trace. The only adjustable parameter here

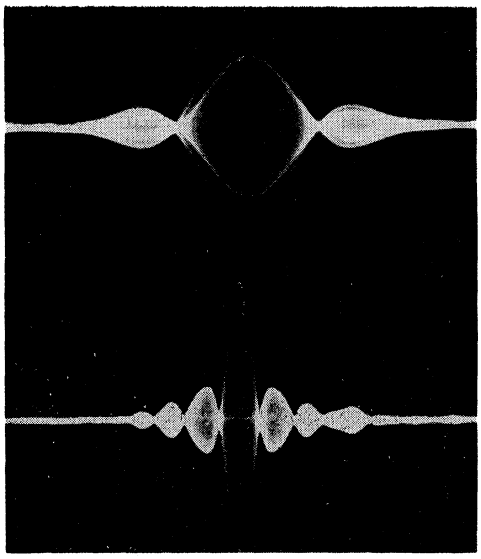

FIG. 12. (a) Photograph of the two echoes superimposed, in the 90–180–180 scheme, showing decrease in amplitude of second echo. (b) Shape of echo produced by sample cell filled partially by liquid He^3, partially by solid. The liquid is saturated in this case by repeating the 90–180–180 sequence several times a second. If we then wait until the liquid has recovered its full moment (5 min) the first echo thereafter has the shape shown in (a), although the sample is partly liquid and partly solid. Sweep speed in both pictures 100 μsec/cm.

is the gradient, G, which is determined by the requirement that γGrt have the value 3.73 at the observed time of the minimum. G thus has the value for this run of 4.12 gauss/cm, which agrees well with that obtained by direct measurement of the field using a proton resonance probe. The agreement between theoretical and experimental line shapes is considered satisfactory, especially in view of the following: I. The gradient has been assumed to be uniform over the volume of the sample. The gradient actually varies from point to point in the magnet, ranging from 3.0 to 4.2 gauss/cm, depending on the particular position the sample cell occupies. The gradient is redetermined upon each reassembly or other mechanical change in the apparatus. II. The ratio $a=r_2/r_1$ is 0.340 for the particular

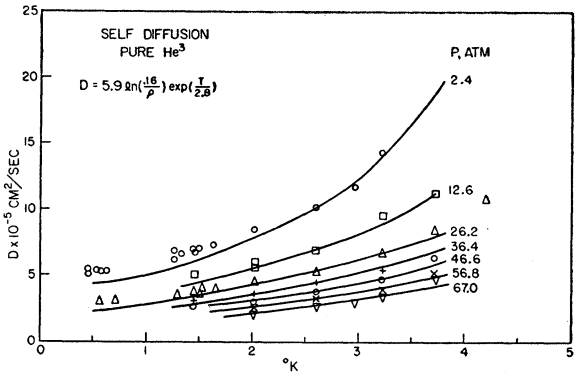

FIG. 13. Diffusion coefficient D *vs* temperature for various pressures in pure liquid He^3. The curves are obtained by plotting log$D$ *vs* T at constant density, using the extensive tables of R. H. Sherman and F. J. Edeskuty (private communication). The points are systematically higher than the curves at the lowest temperatures, but the data are fitted to within experimental accuracy by the equation shown between ~1.5°K and 4°K. No theoretical significance is to be attached to the form of the equation.

sample cell used, and hence the neglected volume is not inappreciable. III. The rf magnetic field (H_1) is not exactly uniform over the volume of the sample, since the filling tube ends just past the edge of the sphere. The measurements of D, T_1, and T_2 do not depend on the echo shape.

The echo shape is the same [Fig. 12(a)] when the cell is filled with solid as it is with liquid, but a cell partially filled with solid He^3 can be made to yield the different shape of Fig. 12(b), as follows: One saturates the liquid ($T_1\sim100$ sec) and then looks at the echo due to the solid ($T_1\sim0.3$ sec). This echo shape is the Fourier transform of a different spin population $n(\omega)$, since the solid is presumed to be in the form of a rather thin shell. It will be seen also that the echo shape shows that the spin relaxation is a bulk phenomenon.

Figure 10 shows the decay of h_2/h_1 predominantly due to diffusion damping as expressed by Eq. (3). The good fit is typical of our liquid results. The same gradient in the solid gives damping due to diffusion only at much longer times, at which the T_2 decay is already appreciable.

V. RESULTS AND DISCUSSION

A. Pure He^3 Liquid

The plots of D as a function of specific volume at constant temperature T, and of D and T_1 as a function of temperature at constant pressure, are shown in Figs. 13–18 for pure He^3 and for He^3 in dilute solution in He^4. There has been some question whether the spin relaxation might be a surface effect, due to oxygen gas condensed onto the surface of the sample cavity. That this cannot be so is shown by the fact that the echo shape is preserved even at short times after saturation, for instance, at $0.01T_1$, when observed with scope sensitivity increased one hundred times, whereas if the

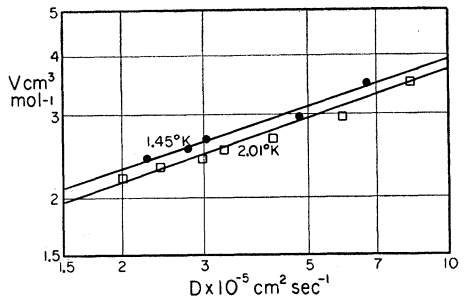

FIG. 14. Specific volume *vs* diffusion coefficient; log$V$ *vs* log$D$.

relaxation occurred at the surface, the short-time echo would be more wiggly (shell-like). One might say then that the wall relaxation was weak, requiring many cross-sample diffusings of a He^3 atom for it to be relaxed —that this is not true is easily shown by observing that with the measured D we can compute the time required for diffusion of an atom to the surface and find it considerably longer for pure He^3 than the measured T_1, indicating that most of the atoms cannot reach the surface even once in a relaxation time, *a forteriori* not the many times required to have surface relaxation masquerade as a homogeneous relaxation under the vigorous test of inspection of the shape of the 1% recovered echo. The decay time for the lowest space mode in a sphere whose surface is black for spin relaxation is, of course, $\tau=R^2/\pi^2D$ with R the sphere radius and D the diffusion coefficient. For our geometry the ratio of the decay time for the lowest mode to that for a sphere was determined by measuring the cooling curve for a billiard ball immersed in running water, then the cooling curve for the same sphere with a hole bored through it. For our geometry we find, then, $\tau=R^2/30D=3.3\times10^{-3}/D$ seconds.

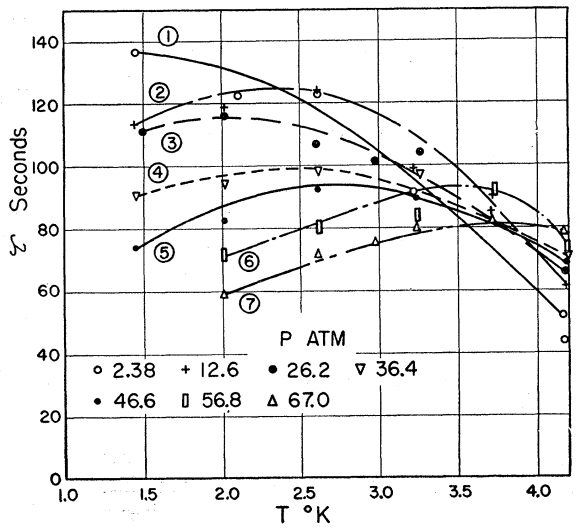

FIG. 15. Relaxation time T_1 in pure liquid He^3 *vs* temperature, pressure as a parameter.

Thus for $D<3\times10^{-5}$ in Fig. 13, relaxation by the walls cannot be faster than 110 seconds. For such D's the T_1's are all smaller than this value, and we see that our nuclear spin relaxation is at least in part a bulk phenomenon. On the other hand, Careri[23] has found that surface relaxation may be induced by packing a sample cell with glass fibers, in the same temperature and pressure range that we operate, although at a different magnetic field. The quality of our relaxation data is markedly inferior to that of the diffusion data, presumably because of the accidental presence of oxygen, which has a well-known strong paramagnetic relaxation effect.

From Fig. 13 it is apparent that the diffusion of atoms in He^3 liquid is not a thermally-activated process —in fact all the curves are very flat below 1.5°K and extrapolate to 0°K at finite (and large) diffusion coefficients. Thus the diffusion process is not that of an ordinary liquid in which the probability of occurrence on a single atom of energy sufficient to surmount the average potential barrier between neighbors (and also the probability of occurrence of low barrier heights) goes like $\exp(-\Delta E/kt)$ where ΔE is the "activation energy" for diffusion. Nor is the diffusion like that of a gas, for which the diffusion coefficient $(D=\lambda\bar{v}/3)$ according to kinetic theory goes like $T^{\frac{1}{2}}$, the independent molecules scattering each other with a cross section

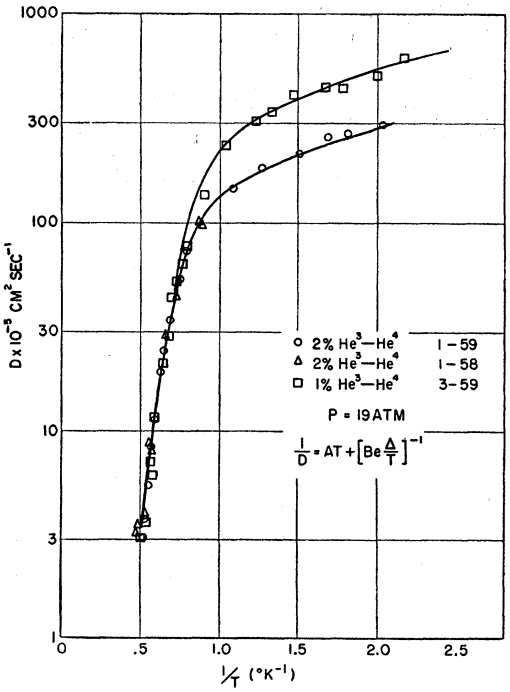

FIG. 16. Log$D$ *vs* $1/T$ for 1% and 2% solutions of He^3 in He^4. The data for 2 atmos and 2% mixture are not shown, for clarity, but they can be fitted by the same form (see Fig. 17). Values of A, B, and Δ are given in the text.

[23] Careri, Modena and Santini, Nuovo cimento (to be published).

more or less independent of energy while the mean velocity of the molecules is $T^{\frac{1}{2}}$. On the other hand, the diffusion of He^3 can be qualitatively understood in terms of the zero-point energy of the individual particles and the tunneling of the atoms through the potential barriers. These are single-particle approximations and surely do not allow an accurate picture of the diffusion mechanism, but the accurate experimental results should provide a test of the validity of the more sophisticated theories, allowing an interpretation at low temperatures as a scattering of the atoms near the Fermi surface by the few thermally excited holes and He^3 atoms.

The classic treatment (6) of spin relaxation gives approximately the following results which are essential to an understanding of our experimental relaxation times:

$$\frac{1}{T_1}\cong 0.3\gamma^4\hbar^2 b^{-6}\left[\frac{\tau_c}{1+\omega_0^2\tau_c^2}+\frac{2\tau_c}{1+4\omega_0^2\tau_c^2}\right], \tag{6}$$

where γ is the gyromagnetic ratio, b the average inter-spin distance, and τ_c the "correlation time" of the motion. ω_0 is the precession frequency in the field H_0, ($\omega_0=\gamma H_0$). This formula is obtained by calculating the amplitude of Fourier component of the perturbing field at ω_0. For $\omega_0\tau_c\ll 1$ this yields approximately

$$1/T_1=\gamma^4\hbar^2 b^{-6}\tau_c=1/T_2. \tag{7}$$

For $\omega\tau_c\gg 1$ we have from (6)

$$1/T_1=\gamma^4\hbar^2 b^{-6}(1/2\omega_0^2\tau_c), \tag{8}$$

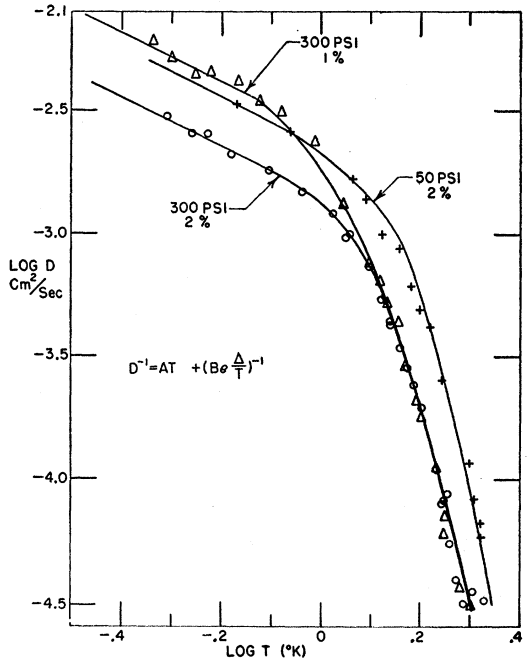

FIG. 17. Log$D$ *vs* log$T$ for various concentrations and pressures, showing the $1/T$ behavior at low temperatures, where the diffusion is limited by He^3-He^3 scattering.

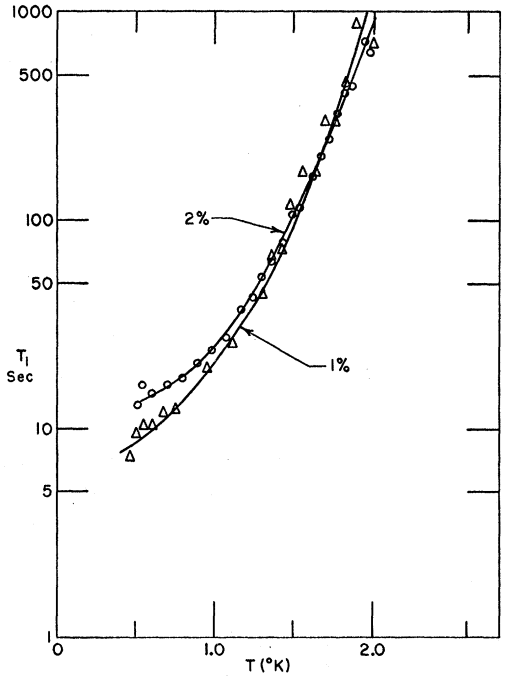

FIG. 18. Relaxation time T_1 for various concentrations of He^3 in He^4 at the same pressures as in Fig. 17.

and

$$1/T_2=0.5\gamma^2\hbar b^{-3}=\tfrac{1}{2}(2\omega_0^2\tau_c/T_1)^{\frac{1}{2}}. \tag{9}$$

The authors of reference 6 have also specialized their treatment to the case of liquids with diffusion coefficient D, in which case for atoms at distance r,

$$\tau_c(r)=r^2/12D \tag{10}$$

and the average over all r from the atom size, a, to infinity gives

$$1/T_1=\gamma^4\hbar^2 N_0/aD, \tag{11}$$

with N_0 the number of magnetic moments per unit volume, for the usual case with $\omega_0\tau_c\ll 1$. In our case, of course, we always have the de Broglie wavelength, λ, much larger than the radius of the atom, so that (11) becomes $1/T_1=\gamma^4\hbar^2 N_0/\lambda D$.

Since we have in the present experiment measured D directly, we can calculate the order of magnitude for T_1 from (11) in the case that D is high enough for $\omega_0\tau_c\ll 1$. If we take for He^3 at reasonable pressure $N_0=2\times 10^{22}$ cm^{-3} and $D=2\times 10^{-5}$ cm^2 sec^{-1} then we calculate (with $a=3\times 10^{-8}$ cm), $T_1\simeq 200$ seconds, in reasonably good agreement with the measured value. A comparison of Fig. 15 with Fig. 13 shows that the diffusion coefficient is a much stronger function of temperature than is the relaxation time T_1, and in fact varies with temperature in the opposite direction, although the discrepancy is not serious since the value of (a) in (11) also changes with temperature. The qualitative agreement of the computed value for T_1 with the measured value must be regarded as satis-

factory and (10) indicates that $\tau_c \lesssim 10^{-10}$ sec so that at our $\omega_0 = 3\times 10^7$ we certainly have $\omega_0\tau_c \ll 1$. Thus one expects from (7) that $T_2 \simeq T_1$ and both should be independent of magnetic field.

B. Pure He^3 Solid

We shall present our results on the solid in a later publication, but it should be noted that the diffusion coefficient is 10^{-3} that of the liquid at the melting pressure even at high temperatures and decreases rapidly with decreasing temperature, leading to shortened and presumably field-dependent T_1 at the lower temperatures.

C. 2% He^3 in He^4 Liquid

Figures 16 and 17 show the rapid rise in diffusion coefficient for 2% He^3 in He^4 with decreasing temperature below the λ point. This lends credence to our regarding the He^4 at low temperatures as analogous to the vacuum of quantum electrodynamics, its function being only to dissolve He^3 and to allow us to work with a He^3 gas of variable density and thus of variable degeneracy temperature. There are, of course, excitations possible in the He^4 liquid and in Fig. 16 we see the freezing out of one type of these excitations (the rotons) with an activation energy near 13.5°K. In sufficiently dilute solutions the He^3 diffusion at low temperature would be limited by He^3-phonon scattering, predicted[9] to give $D \propto T^{-3}$, but the $D \propto (1/T)$ region has much too small a D to be caused by phonon scattering and must be ascribed to a He^3—He^3 transport cross section at 0.5°K of $\simeq 3\times 10^{-15}$ cm^2, the corresponding transport mean free path being about 6 He^3—He^3 distances in the mixture. A temperature-independent scattering cross section in a nondegenerate gas would correspond to $D \propto T^{\frac{1}{2}}$ as computed also by Abrikosov and Khalatnikov[9] and Zharkov and Khalatnikov,[24] but the degeneracy temperature of an ideal Fermi gas of number density corresponding to 2% He^3 in He^4 and of mass 3 is 0.6°K, so that we may very easily be seeing here the diffusion coefficient of a partially degenerate gas, which point will be resolved by measurements at lower temperatures to be obtained with adiabatic demagnetization. At lower temperatures the diffusion coefficient is expected to rise as the longer He^3 wavelength averages over more He^3 scatterers.

It is not clear from Fig. 16 whether D is continuous at $T = T_\lambda$ or not. This is of some interest and will be pursued further. Our value for D at 1.5°K is about a factor 10 below that of Beenakker,[25] but this is successfully accounted for if we extrapolate our results to atmospheric pressure. Our activation energy for rotons is 50% higher than the value usually obtained from thermal data, while Meyer and Reif[26] find 8.3°K for the activation energy of scatterers of positive ions in He II. Their data are of accuracy comparable to ours and the cause of the discrepancy is not known to us. At 1.5°K our D for 2% He^3 is 2×10^{-4} cm^2/sec while the Einstein relation $D = (kT/e)\mu$ gives for Meyer and Reif's positive ions $D = 0.5\times 10^{-4}$ cm^2/sec, a factor four smaller than our value. This large scatter cross section is perhaps an indication of the large size of the ion complex as compared with the small size of the He^3. If one plots the Khalatnikov kinetic coefficients $\bar{B}$ and $\bar{C}$[27] derived by Bendt *et al.*[28] by dividing measured values of viscosity and thermal conductivity by integrals over the experimental excitation spectrum of He II, one finds "activation energies" of 12.1° and 13.5°K for the mean excitation scattering involved in viscosity and thermal conductivity respectively. There is thus implied both by our He^3-roton results and by the viscosity and thermal conductivity measurements a consistent but large variation of roton scattering cross section with temperature.

The relaxation data of Fig. 18 should in principle be computable from the diffusion coefficient of Figs. 16 and 17 by the use of Eqs. (7), (8), (9), and (11). Taking an independent-particle diffusion model we can calculate from (10) the correlation time as at most 5×10^{-11} sec near T_λ, decreasing rapidly below T_λ. Then (11) should give $T_1 \propto D$ whereas a comparison of Figs. 18 and 16 shows T_1 *decreasing* rapidly as D *increases*. This behavior would be expected if the correlation time decreased as expected with increased diffusion coefficient, but the absolute magnitude of correlation time were very long just below T_λ, so that $\omega_0\tau_c \gg 1$. Such a case can be reconciled with the large diffusion coefficient only by assuming clustering of He^3 atoms. T_1 would then vary inversely as magnetic field, and T_2 from (9) would necessarily be much less than $(T_1/\omega)^{\frac{1}{2}}$, i.e. $T_2 < 5\times 10^{-3}$ sec, whereas T_2 is observed to be much longer than 0.2 second. Thus there is some question as to the cause of the spin relaxation in the roton range in dilute solutions of He^3 in He^4.

Since at 0.5°K the time required for the decay of the lowest space mode of the saturated spin system would be ~1 second if the walls were perfectly black, the observed relaxation thus would be obtained if the wall uniformly required $\sim 10^6$ collisions to relax a He^3 spin (see Appendix A). Our present signal-to-noise ratio is not sufficient to allow us to discriminate against wall relaxation which has been demonstrated for certain surfaces by Fairbank[29] and Careri.[23] Akhiezer and Aleksin[30] compute the spin relaxation time T_1 for dilute

[24] V. N. Zharkov and I. M. Khalatnikov, Doklady Akad. Nauk S.S.S.R. **93**, 1007 (1953); I. M. Khalatnikov and V. N. Zharkov, J. Exptl. Theoret. Phys. U.S.S.R. **32**, 1108 (1957) [translation: Soviet Phys. JETP **5**, 905 (1958)].

[25] Beenakker, Taconis, Lynton, Dokoupil, and Van Soest, Physica **18**, 433 (1952).

[26] L. Meyer and F. Reif, Phys. Rev. **110**, 279 (1958).

[27] I. M. Khalatnikov, Uspekhi. Fiz. Nauk **59**, 673 (1956).

[28] Bendt, Cowan, and Yarnell, Phys. Rev. **113**, 1386 (1959).

[29] R. H. Romer and W. M. Fairbank, Bull. Am. Phys. Soc. **4**, 150 (1959).

[30] A. Akhiezer and V. Aleksin, Doklady Akad. Nauk S.S.S.R. **92**, 259 (1953) (National Science Foundation NSF-tr-183).

solutions of He^3 in He^4 and obtain a relaxation time $T_1 \propto T^{-\frac{1}{2}}$ well above the degeneracy temperature and $T_1 \propto T^{-2}$ for the fully degenerate solution. Their high-temperature computation is certainly wrong since they considered the He^3 as an ideal gas, whereas the relaxation rate is very strongly enhanced by the frequent collisions with rotons which serve to increase greatly the correlation time. Their calculation gives for the fully degenerate gas at 0.5°K, $T_1=16$ hours, whereas we find $T_1 \simeq 30$ sec.

We have also measured D in 1% He^3 in He^4 at 19 atmos and in 2% He^3 in He^4 at 2 atmos to see whether (a) the $D \propto 1/T$ behavior at low temperatures is He^3-He^3 scattering and (b) whether the 13.5° "activation energy" is concentration dependent. The diffusion data may be fitted with an equation of the form $D^{-1}=AT+[B\exp(\Delta/T)]^{-1}$. For the 2% mixture at 19 atmos, $A=719$, $B=4.17\times10^{-8}$, and $\Delta=13.7$°K. For the 1% mixture at the same pressure, $A=382$, $B=4.5\times10^{-8}$, and $\Delta=12.9$°K, thus demonstrating that the $1/T$ behavior below 1°K is indeed He^3-He^3 scattering in the He^4 "vacuum." The 2-atmos curve for 2% He^3 is similar to that at 19 atmos, except for the pressure shift in the λ point. The difference between the Δ's for the 1% and 2% mixtures is not regarded as significant.

VI. WORK IN PROGRESS

Measurements are being made on the susceptibility of dilute solutions and on the solid, on the diffusion coefficient and relaxation times T_1 and T_2 to 0.01°K, and on the field dependence of T_1, especially in the solid. With the onset of complete degeneracy in the solid and in dilute solutions, and with the disappearance of excitations in the pure liquid, interesting qualitative results should be obtainable.

VII. ACKNOWLEDGMENTS

We wish to thank P. J. Maloney and A. M. Patlach for assistance in apparatus design and construction, and G. Present and Miss. A. Willner for measurement of the photographic records. Miss Willner also coded the 650 computer and performed the many computations involved.

APPENDIX A

The relationship between macroscopic "wall relaxation" and the microscopic nature of the wall collisions is an interesting one. For example, let us take a case in which the mean free path of the fluid atoms is large compared to the range of magnetic interaction of particles with the wall. If the probability of relaxation due to paramagnetic adsorbents, etc, in a single collision with the wall is ϵ, then we may estimate the expected relaxation time τ. Suppose the sample cell to be compact, of volume V and surface S. Let there be n atoms per cc with thermal velocity v and mean-free-path λ. Then there will be $\sim nv/4$ atoms per second

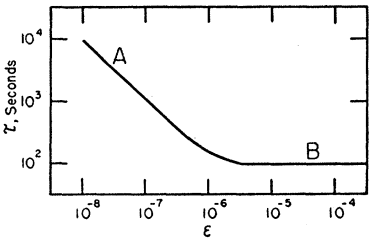

FIG. 19. τ *vs* ϵ showing relaxation limited by (A) wall collisions and (B) by diffusion.

incident on each cm^2 of wall; i.e., $nvS/4$ wall collisions per unit time. If the wall relaxation is very weak—i.e., $\epsilon \to 0$, then this means that in a completely saturated sample $nvS\epsilon/4$ spins are relaxed per second, giving

$$\tau=\frac{nV}{nvS\epsilon/4}=\frac{1}{\epsilon v}\frac{4V}{S}. \tag{A}$$

This can only be true, however, if the τ so calculated is long compared with the decay time τ_D for the lowest space mode of the diffusion equation $[\tau_D \simeq 1/D(V/S)^2]$. For $\epsilon > \epsilon_{crit}$, where $\epsilon_{crit} \equiv 4SD/Vv$, the relaxation time τ will become constant at $\tau \simeq \tau_D$. The relaxation will be slightly nonexponential, most strikingly in that the relaxation rate at late times will extrapolate to a nonzero moment at zero time. Thus the relation between τ and ϵ is that shown in Fig. 19, which has been calculated for $V=1$ cm^3, $S=3$ cm^2, $v=10^4$ cm/sec, $\lambda=3\times10^{-7}$ cm.

In case one finds experimentally that $\tau=\tau_D$, one can distinguish between wall relaxation and bulk relaxation because a perfectly "black wall" evidently will produce an initial rate of change of total magnetization proportional to $t^{-\frac{1}{2}}$, and a total recovered magnetization which is proportional to $t^{\frac{1}{2}}$, as is characteristic of heated bodies subjected to sudden jumps in surface temperature. With $\epsilon=1$ this behavior will indeed be observed, but in cases where $1>\epsilon>10^{-6}$, all of which give $\tau=\tau_D$, the evidence would not be so clear. In this case the rate of flow of relaxation into the sample is

$$\dot{R}=\frac{\epsilon nvS}{4nV}(1-r),$$

where R is the fraction of total magnetic moment recovered, averaged over the volume, and r is the local value at the surface. For $\epsilon<1$, $r=0$ at $t=0$ and we have

$$\dot{R}(0)=\frac{\epsilon nvS}{4nV}.$$

Thus

$$\tau\dot{R}(0) \simeq \tau_D\dot{R}(0) \simeq \frac{\epsilon vS}{4VD}\left(\frac{V}{S}\right)^2 \simeq \frac{\epsilon Vv}{4DS} \simeq \frac{\epsilon}{\epsilon_{crit}}, \tag{B}$$

and we see that the initial rate of recovery of a sample relaxed by gray walls is larger by a factor ϵ/ϵ_{crit} than that which corresponds to exponential recovery with

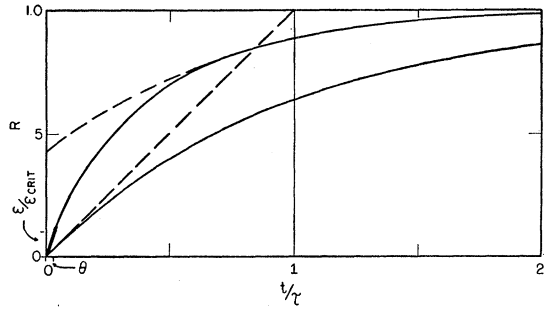

FIG. 20. Diagram showing the departure from exponential recovery, exaggerated.

$\tau=\tau_D$. Indeed, for $\epsilon/\epsilon_{\text{crit}}\gg 1$, this is such a large relaxation rate at the wall that the diffusion away of the relaxed atoms cannot remove all this relaxation and $r\rightarrow 1$ very shortly. In fact, in time θ all atoms to a depth d, where $d^2=\theta D$, are affected reasonably uniformly, since they are mixed by diffusion. In time θ then, relaxation $R=\epsilon\theta/\epsilon_{\text{crit}}\tau_D$ has diffused in (for $1>\epsilon>\epsilon_{\text{crit}}$). The initial high relaxation rate thus continues until $r\simeq 1$, i.e., until

$$r\equiv\frac{(\epsilon/\epsilon_{\text{crit}})(\theta/\tau_D)}{dS/V}\simeq 1.$$

The high relaxation rate continues until $\theta=\tau_D(\epsilon_{\text{crit}}/\epsilon)^2$ after which time $r\simeq 1$ near the wall and the relaxation becomes indistinguishable from that due to a black wall. Thus R will behave as in Fig. 20.

To estimate the possibilities of detecting such uniform wall relaxation effects, we note from the above that relaxation at the initial rate continues until $\epsilon_{\text{crit}}/\epsilon$ of the sample has been relaxed, after which the recovery is slower, like $t^{\frac{1}{2}}$, until the diffusion front covers a considerable part of the sample, say to time $\tau_D/2$, after which the recovery is exponential with characteristic time τ_D, but with a considerable recovered moment extrapolated to zero time. So we see that for most of the range of ϵ for which wall relaxation is independent of ϵ, even the details of the relaxation *vs* time are ϵ-independent, and are just about what one would expect from a black wall. To distinguish ϵ from unity requires investigation of the first $(\epsilon_{\text{crit}}/\epsilon)\tau$ seconds of the recovery. On the other hand, uniform wall relaxation with $\tau=\tau_D$ has a much greater initial recovery rate than the bulk exponential and so is clearly distinguishable from it.

Of course, the relevance of this simple example is much diminished by the formation of "liquid crystals" near the wall, and the concomitant increased relaxation rate seen even near an inert wall, and by any magnetic nonuniformity of the wall itself. However, the analysis may be of some general interest.

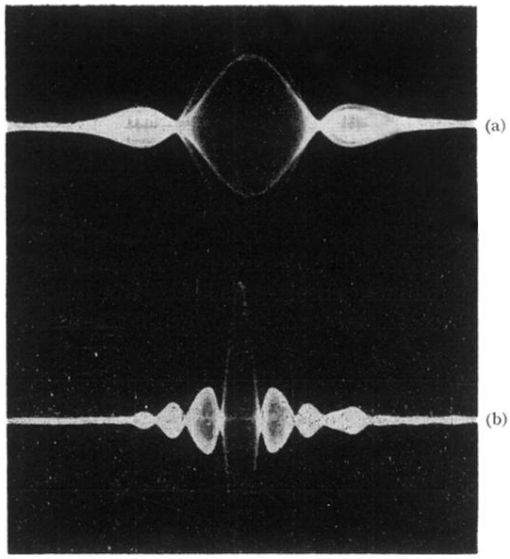

FIG. 12. (a) Photograph of the two echoes superimposed, in the 90–180–180 scheme, showing decrease in amplitude of second echo. (b) Shape of echo produced by sample cell filled partially by liquid He^3, partially by solid. The liquid is saturated in this case by repeating the 90–180–180 sequence several times a second. If we then wait until the liquid has recovered its full moment (5 min) the first echo thereafter has the shape shown in (a), although the sample is partly liquid and partly solid. Sweep speed in both pictures 100 μsec/cm.

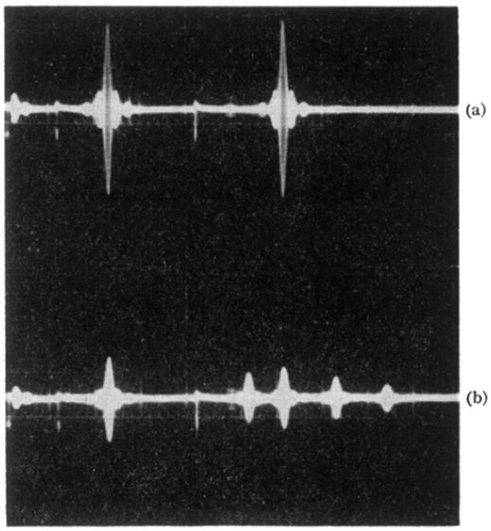

FIG. 9. (a) Photograph of spin echoes resulting from 90–180–180 sequence. The second echo is not much damped by diffusion. (b) Photograph of spin echoes from same pulse sequence as in (a) but with 180 pulse amplitude reduced by half. Notice the diminution of echo amplitude, as well as the appearance of three extra echoes. Sweep speed in both pictures is 1 msec/cm.